Diruthenium Tetraacetate Monocation, [Ru$^{II/III}_2$(O$_2$CMe)$_4$]$^+$, Building Blocks for 3-D Molecule-Based Magnets

Thomas E. Vos,[†] Yi Liao,[†] William W. Shum,[†] Jae-Hyuk Her,[‡] Peter W. Stephens,[†] William M. Reiff,[§] and Joel S. Miller*,[†]

Contribution from the Department of Chemistry, University of Utah, 315 S. 1400 E. RM 2124, Salt Lake City, Utah 84112-0850; Department Physics and Astronomy, State University of New York, Stony Brook, New York 11794-3800; and Department of Chemistry and Chemical Biology, Northeastern University, 360 Huntington Avenue, Boston, Massachusetts 02115

Received March 31, 2004; E-mail: jsmiller@chem.utah.edu

Abstract: Diruthenium tetracarboxylates monocations are utilized as building blocks for cubic 3-D network structured molecule-based magnets. [Ru$^{II/III}_2$(O$_2$CMe)$_4$]$_3$[M^{III}(CN)$_6$] [M = Cr (**1a**), Fe (**2**), Co (**3**)] were prepared in aqueous solution. Powder X-ray diffraction indicates that they have body-centered cubic structures (space group = $Im\bar{3}m$, a = 13.34, 13.30, and 13.10 Å for **1a**, **2**, and **3**, respectively), which was confirmed for **1a** by Reitveld analysis of the synchrotron powder data [a = 13.3756(5) Å]. [Ru$_2$(O$_2$CMe)$_4$]$_3$[M^{III}(CN)$_6$]·xMeCN [M = Cr, x = 1.8 (**1b**); M = Mn, x = 3.3 (**4**)] were prepared from acetonitrile. The magnetic ordering of **1a** (33 K), **1b** (34.5 K), **2** (2.1 K), and **4** (9.6 K) was determined from the temperature dependencies of the in-phase (χ') alternating current (AC) susceptibility. The field dependence of the magnetization, $M(H)$, at 2 K for **1a** showed an unusual constricted hysteresis loop with a coercive field, H_{cr}, of 470 Oe while the $M(H)$ data for **1b**, **2**, and **4** showed a normal hysteresis loop with a coercive field of 1670, 10, and 990 Oe, respectively. The ^{57}Fe Mössbauer spectrum of **2** is consistent with the presence of low spin Fe^{III} (δ = −0.05 mm/s; ΔE = 0.33 mm/s) at room temperature, and the onset of 3-D magnetic ordering at lower temperature (<2 K). The effects of M^{III} in [M^{III}(CN)$_6$]$^{3-}$, and the large zero-field splitting (D) of diruthenium tetracarboxylates are discussed. The increasing critical temperatures T_c, with increasing S could not be accounted for by mean field models without significantly different J values for **1a**, **4**, and **2**. By fitting the T_c data with mean field models [**H** = $-2JS_{Ru}\cdot S_M - \mu_B(g_{Ru}S_{Ru} + g_M S_M)H$], J/k_B are 4.46, 1.90, and 0.70 K for **1a**, **4**, and **2**, respectively.

Introduction

The development of molecule-based magnetic materials has made significant progress with a broad array of building blocks being utilized.[1] Recently, our group initiated a project to incorporate diruthenium tetracarboxylate monocations, [Ru$^{II/III}_2$-(O$_2$CR)$_4$]$^+$, into a 3-D network Prussian blue-like structure to form a magnetically ordered materials,[2] while Yoshioka et al. reported the crystal structure and paramagnetic properties of 2-D [Ru$_2$(piv)$_4$]$_3$[Fe^{III}(CN)$_6$]·4H$_2$O (Hpiv = pivalic acid).[3]

D_{4h} [Ru$^{II/III}_2$(O$_2$CR)$_4$]$^+$ has a $\sigma^2\pi^4\delta^2\delta^{*1}\pi^{*2}$ $S = {}^3/_2$ valence electronic configuration.[4,5] Consequently it an is unusually high spin for a second row coordination complex. Additionally, these tetracarboxylates have an unusually large zero-field splitting,

D (+63 ± 11 cm^{-1}).[5b,6,7] Hence, materials based upon such building blocks were anticipated to exhibit atypical magnetic properties. Several extended structures based on their ability of the cation to add one or two ligands axial to the RuRu bond have been reported.[8,9,10] However, when diruthenium tetracarboxylates were bridged with organic radicals, such as nitroxides,

† University of Utah.
‡ State University of New York.
§ Northeastern University.

(1) (a) Ovcharenko, V. I.; Sagdeev, R. Z. *Russ. Chem. Rev.* **1999**, *68*, 345−363. (b) Day, P. *J. Chem. Soc., Dalton Trans.* **1997**, 701−706. (c) Miller, J. S.; Epstein, A. J. *Chem. Eng. News* **1995**, *73* (40), 30−41. Miller, J. S.; Epstein, A. J. *Adv. Chem. Ser.* **1995**, *245*, 161−181. (d) Miller, J. S.; Epstein, A. J. *Chem. Commun.* **1998**, 1319−1325. (e) Miller, J. S.; Epstein, A. J. *Angew. Chem., Int. Ed. Engl.* **1994**, *33*, 385−415.
(2) Liao, Y.; Shum, W. W.; Miller, J. S. *J. Am. Chem. Soc.* **2002**, *124*, 9336−9337.
(3) Yoshioka, D.; Mikuriya, M.; Handa, M. *Chem. Lett.* **2002**, *31*, 1044−1045.
(4) Cotton, F. A.; Walton, R. A. *Multiple bonds between Metal Atoms*, 2nd ed.; Clarendon Press: Oxford, U.K., 1993; p 18.

(5) (a) Norman, J. G., Jr.; Renzoni, G. E.; Case, D. A. *J. Am. Chem. Soc.* **1979**, *101*, 5256−5257. (b) Miskowiski, V. M.; Hopkins, M. D.; Winkler, J. R.; Gray, H. B. In *Inorganic Electronic Structure and Spectroscopy*; Solomon, E. I.; Lever, A. B. P., Eds.; John Wiley & Sons: 1999; Vol. 2, Chapter 6.
(6) (a) Telser, J.; Drago, R. S. *Inorg. Chem.* **1985**, *24*, 4765. (b) Telser, J.; Drago, R. S. *Inorg. Chem.* **1984**, *23*, 3114−3120. (c) Cukiernik, F. D.; Giroud-Godquin, A. M.; Maldivi, P.; Marchon, J. C. *Inorg. Chim. Acta* **1994**, *215*, 203−207. (d) Handa, M.; Sayama, Y.; Mikuriya, M.; Nukada, R.; Hiromitsu, I.; Kasuga, K. *Bull. Chem. Soc. Jpn.* **1998**, *71*, 119−125. (e) Jimenez-Apraricio, R.; Urbanos, F. A.; Arrieta, J. M. *Inorg. Chem.* **2001**, *40*, 613−619.
(7) Cukiernik, F. D.; Luneau, D.; Marchon, J. C.; Maldivi, P. *Inorg. Chem.* **1998**, *37*, 3698−3704.
(8) Beck, E. J.; Drysdale, K. D.; Thompson, L. K.; Li, L.; Murphy, C. A.; Aquino, M. A. S. *Inorg. Chim. Acta* **1998**, *279*, 121−125.
(9) (a) Cotton, F. A.; Lu, J.; Yokochi, A. *Inorg. Chim. Acta* **1998**, *275−276*, 447−452. (b) Cotton, F. A.; Kim, Y.; Ren, T. *Inorg. Chem.* **1992**, *31*, 2723−2726. (c) Cotton, F. A.; Kim, Y.; Ren, T. *Polyhedron* **1993**, *12*, 607−611. (d) Cotton, F. A.; Matusz, M.; Zhong, B. *Inorg. Chem.* **1988**, *27*, 4368−4372.
(10) (a) Handa, M.; Sayama, Y.; Mikuriya, M.; Nukada, R.; Hiromitsu, I.; Kasuga, K. *Chem. Lett.* **1996**, 201−202. (b) Sayama, Y.; Handa, M.; Mikuriya, M.; Hiromitsu, I.; Kasuga, K. *Chem. Lett.* **1998**, 777−778. (c) Handa, M.; Sayama, Y.; Mikuriya, M.; Nukada, R.; Hiromitsu, I.; Kasuga, K. *Bull. Chem. Soc. Jpn.* **1995**, *68*, 1647−16753.
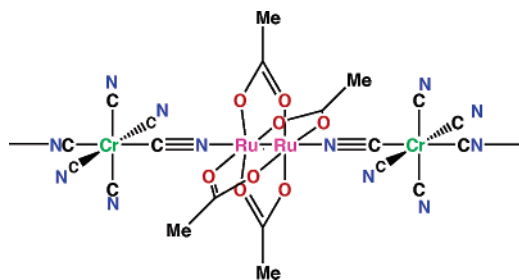
Figure 1. [Ru$^{II/III}$$_2$(O$_2$CR)$_4$]$^+$ bonding to two [Cr^{III}(CN)$_6$]$^{3-}$ via trans cyanides, and each [Cr^{III}(CN)$_6$]$^{3-}$ can bond to six cations.

albeit antiferromagnetically coupled, magnetic ordering does not occur.[10a,b] Herein, we report [Ru$^{II/III}$$_2$(O$_2$CR)$_4$]$^+$ linked by [M^{III}(CN)$_6$]$^{3-}$ (M = Cr, Mn, Fe, Co) that form 3-D magnetic materials. Each [Cr^{III}(CN)$_6$]$^{3-}$ can bond to six [Ru$^{II/III}$$_2$(O$_2$CR)$_4$]$^+$, which itself can bond to two [Cr^{III}(CN)$_6$]$^{3-}$, Figure 1. Hence, this arrangement leads to a [Ru$^{II/III}$$_2$(O$_2$CR)$_4$]$_3$[Cr^{III}(CN)$_6$] charge-compensated stoichiometry. This structure makes [Ru$^{II/III}$$_2$-(O$_2$CR)$_4$]$^+$ an air-stable analogue of V^{2+} ion, e.g., cubic V^{II}$_3$[Cr^{III}(CN)$_6$], a room-temperature molecule-based magnet.[11] Herein, we report a systematic study of utilizing diruthenium tetracarboxylates for molecule-based magnets. [Ru$_2$(O$_2$CMe)$_4$]$_3$[M^{III}(CN)$_6$] [M = Cr (**1a**), Fe (**2**), Co (**3**)] were prepared in aqueous solution, while [Ru$_2$(O$_2$CMe)$_4$]$_3$[M^{III}(CN)$_6$]·xMeCN [M = Cr, x = 1.8 (**1a**); M = Mn, x = 3.3 (**4**)] were prepared in acetonitrile.

Experimental Section

[Ru$_2$(O$_2$CMe)$_4$]Cl,[12] [Ru$_2$(O$_2$CMe)$_4$(H$_2$O)$_2$][BPh$_4$],[13] [(Ph$_3$P)$_2$N]$_3$[Mn-(CN)$_6$],[14] [(Ph$_3$P)$_2$N]$_3$[Cr(CN)$_6$],[14] K$_3$[Cr(CN)$_6$],[15] and K$_3$[Co(CN)$_6$][16] were prepared via literature methods, while K$_3$[Fe(CN)$_6$] were used as purchased from Baker. All solvents were used as bought from Fisher Scientific. All operations were carried out in air unless noted. The water was purified by reverse osmosis. Acetonitrile was dried by two activated alumina columns and collected under nitrogen.[17] The solids were isolated on a glass frit with a porosity of 4−5.5 μm or by centrifugation with a Clay-Adams 2 Ampere 115 V Safety-Head Centrifuge for 5 min.

Powder samples for magnetic measurements were loaded in gel-cap holders. The DC magnetization temperature dependence was obtained by cooling in zero field, and then data was collected on warming in 5 or 50 Oe external magnetic field using a Quantum Design MPMS-5XL 5 T SQUID magnetometer equipped with a reciprocating sample measurement system, low field option, and continuous low-temperature control with enhanced thermometry features. Powder X-ray diffraction were made on a Philips X'Pert MPD diffractometer (Cu Kα) using Mica (Standard Reference Material 675) as an internal standard. Additional powder diffraction measurements for Reitveld structure analysis were performed at Beam Line ×3B1 of the National Synchrotron Light Source at Brookhaven National Laboratory. The powdered sample was held in a thin wall glass capillary of nominally

0.5 mm diameter. X-rays of wavelength 0.699 47(2) Å were selected by a Si(111) double crystal monochromator. Diffracted X-rays were selected by a Ge(111) analyzer and detected by a scintillation counter. The incident intensity was monitored by an ion chamber, and the measured signal was normalized. Infrared spectra were recorded between 400 and 4000 cm^{-1} on either a BioRad FTS-40 or a Bruker Tensor 37 spectrometer.

[Ru$_2$(O$_2$CMe)$_4$]$_3$[Fe^{III}(CN)$_6$] used for ^{57}Fe Mössbauer studies were enclosed in a Vespel holder that was sealed with epoxy. The spectra were determined by using a conventional constant acceleration spectrometer operated in multichannel scaling mode. The γ-ray source consisted of a fresh 25 mCi of ^{57}Co in a rhodium metal matrix that was maintained at ambient temperature. The spectrometer was calibrated using a 6-μm thick natural abundance iron foil. Isomer shifts are reported relative to the center of the magnetic hyperfine pattern of the latter foil taken as zero velocity. The line widths of the innermost pair of the $\Delta M = \pm 1$ transitions of the latter Zeeman pattern were reproducibly determined to be 0.214 mm/s. Sample temperature control was achieved using a standard exchange gas liquid helium cryostat (Cryo Industries of America, Inc.) with temperature measurement and control based on silicon diode thermometry in conjunction with a 10-μA excitation source (Lakeshore Cryotronics, Inc.). Spectra were fit to unconstrained Lorentzians using the program ORIGIN (Origin Lab, Inc.).

Microanalyses were performed by Atlantic Microlab, Inc. or Complete Analysis Laboratories, Inc.. The density was determined from the onset of flotation utilizing a CH$_2$I$_2$/CH$_2$Cl$_2$ mixture and weighing a 2.00-mL volume. The thermal properties were studied on a TA Instruments model 2050 thermogravimetric analyzer (TGA) equipped with a TA-MS Fison triple-filter quadrupole mass spectrometer to identify gaseous products with masses less than 300 amu. The TGA was located in a Vacuum Atmospheres DriLab under argon to protect air- and moisture-sensitive samples. Samples were placed in an aluminum pan and heated at 10 °C/min under a continuous 10 mL/min nitrogen flow.

[Ru$_2$(O$_2$CMe)$_4$]$_3$[Cr^{III}(CN)$_6$] (1a). To a solution of 100 mg (0.211 mmol) of [Ru$_2$(O$_2$CMe)$_4$]Cl dissolved in 50 mL of water was added 22.0 mg (0.0676 mmol) of K$_3$[Cr(CN)$_6$] dissolved in 5 mL of water. The resultant mixture was stirred for 1 h. The precipitate was collected and washed with water and dried in air (Yield: 102 mg, 99%). IR 2138 cm^{-1} (ν_{CN}). Calcd for C$_{30}$H$_{36}$CrN$_6$O$_{24}$Ru$_6$: C, 23.66; H, 2.38; N, 5.52. Found: C, 23.82; H, 2.48; N, 5.72.

[Ru$_2$(O$_2$CMe)$_4$]$_3$[Cr^{III}(CN)$_6$]·1.8MeCN (1b). To a 10-mL acetonitrile solution of 50.7 mg (0.076 mmol) of [Ru$_2$(O$_2$CMe)$_4$(THF)$_2$][BF$_4$] cooled to −15 °C in a salt−ice bath was added 48.8 mg (0.026 mmol) of [(Ph$_3$P)$_2$N]$_3$[Cr(CN)$_6$] dissolved in 5 mL of acetonitrile. The solution immediately turned turbid with orange-brown solids. The solution was stirred for an additional 30 min at −15 °C, and then the solids (yield: 30.5 mg, 79%) were isolated by centrifugation and the resulting solution was slightly yellow-orange. IR 2142 cm^{-1} (ν_{CN}). Calcd for C$_{33.6}$H$_{41.4}$-CrN$_{7.8}$O$_{24}$Ru$_6$: C, 25.27; H, 2.61; N, 6.84. Found: C, 25.21; H, 2.59; N, 7.00.

[Ru$_2$(O$_2$CMe)$_4$]$_3$[Fe^{III}(CN)$_6$] (2) was prepared similarly to **1a** except K$_3$[Fe(CN)$_6$] was used (yield: 98 mg, 95%). IR 2116 cm^{-1} (ν_{CN}). Calcd for C$_{30}$H$_{36}$FeN$_6$O$_{24}$Ru$_6$: C, 23.60; H, 2.38; N, 5.50. Found: C, 23.68; H, 2.41; N, 5.14.

[Ru$_2$(O$_2$CMe)$_4$]$_3$[Co^{III}(CN)$_6$] (3) was prepared similarly to **1a** except K$_3$[Co(CN)$_6$] was used (yield: 99 mg, 96%). IR 2125 cm^{-1} (ν_{CN}). Calcd for C$_{30}$H$_{36}$CoN$_6$O$_{24}$Ru$_6$: C, 23.55; H, 2.37; N, 5.49. Found: C, 23.37; H, 2.13; N, 5.28.

[Ru$_2$(O$_2$CMe)$_4$]$_3$[Mn(CN)$_6$]·3.3MeCN (4). All the operations were carried out under a nitrogen atmosphere. **4** was prepared in a similar method as **1b** except that [(Ph$_3$P)$_2$N]$_3$[Mn(CN)$_6$] was used. IR 2118 cm^{-1} (ν_{CN}). When this reaction was run at room temperature, the solution turned purplish black and the solids were black instead of brown; the IR contained broad ν_{CN} bands at 2070 and 2115 cm^{-1}

(11) Ferlay, S.; Mallah, T.; Ouahes, R.; Viellet, P.; Verdaguer, M. *Nature* **1995**, *378*, 701−703.
(12) Mitchell, R. W.; Spencer, A.; Wilkinson, G. *J. Chem. Soc., Dalton Trans.* **1973**, *8*, 846−854.
(13) (a) McCann, M.; Carvill, A.; Cardin, C.; Convery, M. *Polyhedron* **1993**, *12*, 1163−1169. (b) Holmes, S. M.; Girolami, G. S. *J. Am. Chem. Soc.* **1999**, *121*, 5593−5594. (c) Hatlevik, Ø.; Buschmann, W. E.; Zhang, J.; Manson, J. L.; Miller, J. S. *Adv. Mater.* **1999**, *11*, 914−918.
(14) Buschmann, W. E.; Liable-Sands, L.; Rheingold, A. L.; Miller, J. S. *Inorg. Chim. Acta* **1999**, *284*, 175−179.
(15) Alexander, J. J.; Gray, H. B. *J. Am. Chem. Soc.* **1968**, *90*, 4260−4271.
(16) Bigelow, J. H. *Inorg. Synth.* **1946**, *2*, 225−227.
(17) Pangborn, A. B.; Giardello, M. A.; Grubbs, R. H.; Rosen, R. K.; Timmers, F. J. *Organometallics* **1996**, *15*, 1518−1520.
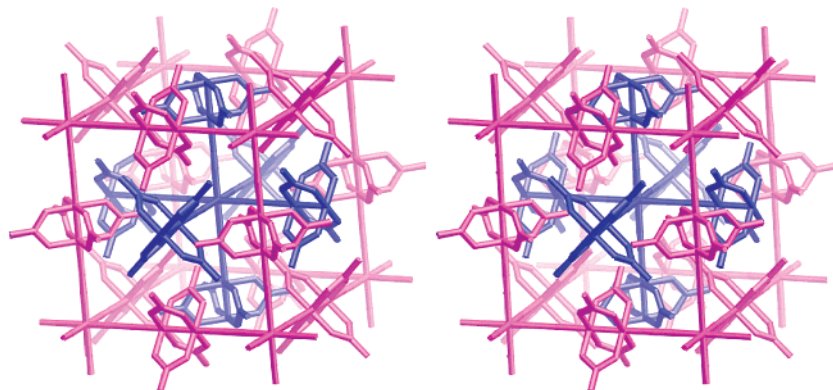
Figure 2. Stereoview of the 3-D body centered cubic structure of **1a** showing the two interpenetrating lattices in blue and pink.

(yield: 26.3 mg, 65%). Calcd for $C_{36.6}H_{45.9}CrN_{9.3}O_{24}Ru_6$: C, 26.46; H, 2.78; N, 7.84. Found: C, 26.27; H, 3.00; N, 8.06.

Results and Discussion

Synthesis and Stability. Air stable $[Ru^{II/III}_2(O_2CMe)_4]_3$-$[M^{III}(CN)_6]$ [M = Cr (**1a**), Fe (**2**), Co (**3**)] were obtained by mixing aqueous solutions of $[Ru^{II/III}_2(O_2CMe)_4]Cl$ and $K_3[M^{III}$-$(CN)_6]$. The υ_{CN} in the IR spectrum is a single sharp absorption at 2138, 2116, and 2125 cm^{-1} for **1a**, **2**, and **3**, respectively, consistent with maintaining octahedral symmetry about the M^{III} site. However, the aqueous method is not applicable to the preparation of $[Ru^{II/III}_2(O_2CMe)_4]_3[Mn^{III}(CN)_6]$ (**4**) because $[Mn^{III}(CN)_6]^{3-}$ is hydrolytically unstable. Hence, **4** was synthesized in acetonitrile from the reaction of $[Ru_2(O_2CMe)_4$-$(THF)_2][BF_4]$ and $[(Ph_3P)_2N]_3[Mn(CN)_6]$. $[Ru_2(O_2CMe)_4]_3[Cr^{III}$-$(CN)_6]$ could also be prepared in acetonitrile except that $[Ru_2(O_2CMe)_4(THF)_2][BF_4]$ and $[(Ph_3P)_2N]_3[Cr(CN)_6]$ were utilized. The IR spectra of **1a** and **1b** are nearly identical except that the IR spectrum of **1b** contains additional peaks associated with MeCN. The υ_{CN} in the IR spectrum is a single sharp absorption at 2142 and 2118 cm^{-1} for **1b** and **4**, respectively.

The stability of the network solids is dependent on the route used to synthesize the compounds. Compounds obtained from aqueous reaction showed no evidence of decomposition in the IR spectrum or magnetic data after 2 months in the air at room temperature. However, compounds prepared from acetonitrile solution are only stable below −20 °C. They decompose slowly at room temperature accompanied with a new broad υ_{CN} absorption at 2090 cm^{-1} and decrease of magnetic ordering temperature. Similar instabilities were noted for some nonaqueous-prepared Prussian blue structured materials.[18] The decomposition appears to be unrelated to air and moisture but correlated with reduced crystallinity. In fact, the products are somewhat more stable in an atmosphere with moisture. Unlike crystalline **1a**, **1b** is amorphous and contains a significant amount of MeCN. The decomposition is correlated to the loss of MeCN from the network structure.

Structure, Density, and Solubility. Based on the stoichiometry and ability of $[Ru_2(O_2CR)_4]^+$ to axially coordinate to two trans cyanide Ns of $[M(CN)_6]^{3-}$, **1** to **4** are proposed to form a 3-D network structure with $-M-C\equiv N-Ru\equiv Ru-N\equiv C-M-$ linkages, Figure 1, along all three Cartesian axes of a cubic unit cell, Figure 2. A related motif is observed for the Prussian blue family of magnetic materials.[11,19]

1a, **2**, and **3** prepared from water are crystalline and have similar powder diffraction patterns. They can be indexed[20] to isomorphous body-centered cubic structures with $a = 13.34$, 13.30, and 13.10 Å, respectively. Based upon structures of $[M(CN)_6]^{3-}$[21] and $[Ru_2(O_2CMe)_4]^+$,[6] the M···M separation, a, is expected to be ~13 Å, and $a_{Co} < a_{Fe} < a_{Cr}$ are expected for the $M-C\equiv N-Ru\equiv Ru-N\equiv C-M$ linkage, as observed.

The body centered cubic crystal structure of **1a** was consistent with the Reitveld analysis of the synchrotron powder diffraction data. Initial estimates of the atomic coordinates were adapted from a similar structure.[7] The Reitveld refinement is shown in Figure 3, and selected diffraction data are given in Table 1.

The Reitveld analysis provided $a = 13.3756(5)$ and CrC, CN, NRu, RuRu, RuO, OC, and CC distances of 2.28(8),[22] 0.93(16), 2.34(10), 2.28(2), 2.03(3), 1.34(6), and 1.38(10) Å, respectively. The body-centered space group indicates a second, independent lattice interpenetrating the primitive lattice, as observed for other compounds, e.g., $Mn[C(CN)_3]_2$.[23] The $[Ru_2(O_2CMe)_4]^+$ paddlewheel is rotated 45° with respect to the octahedral $[M(CN)_6]^{3-}$ in order to accommodate the second, interpenetrating lattice, Figure 2.

Further evidence of a second interpenetrating lattice was obtained from the measured densities of **1a**, **2**, and **3**. The densities of **1a**, **2**, and **3** were determined to be 2.08, 2.16, and 2.18 g cm^{-3}, respectively. These are in good agreement with the calculated densities (2.13, 2.16, 2.26 g cm^{-3}) for body-centered cubic structures and twice that calculated for the primitive cubic structures.

The interpenetrating lattice structure of $[Ru^{II/III}_2(O_2CMe)_4]_3$-$[M^{III}(CN)_6]$ does not contain void space to accommodate water, as observed with no water incorporation in **1a**. Molecular

(18) Buschmann, W. E.; Miller, J. S. *Inorg. Chem.* **2000**, *39*, 2411−2421.

(19) For example, see: (a) Mallah, T.; Thiebaut, S.; Verdaguer, M.; Veillet, P. *Science* **1993**, *262*, 1554. (b) Entley, W. R.; Girolami, G. S. *Inorg. Chem.* **1994**, *33* (3), 5165−5166.

(20) CMPR distributed by NIST: http://webster.ncnr.nist.gov/programs/crystallography/software/cmpr/.

(21) For example, see: (a) Ohba, M.; Usuki, N.; Fukita, N.; Okawa, H. *Inorg. Chem.* **1998**, *37*, 3349−3354. (b) Ferlay, S.; Mallah, T.; Vaissermann, J.; Bartolome, F.; Veillet, P.; Verdaguer, M. *J. Chem. Soc., Chem. Commun.* **1996**, 2481−2482. (c) Re, N.; Crescenzi, R.; Floriani, C.; Miyasaka, H.; Matsumoto, N. *Inorg. Chem.* **1998**, *37*, 2717−2722. (d) Lu, J.; Harrison, W. T. A.; Jacobson, A. J. *J. Chem. Soc., Chem. Commun.* **1996**, 399−400. (e) Ohba, M.; Okawa, H.; Fukita, N.; Hashimoto, Y. *J. Am. Chem. Soc.* **1997**, *119*, 1011−1019.

(22) The esd's given in the atomic coordinates are statistical estimates, taken directly from the output of the Reitveld program (GSAS). It is widely accepted that the accuracy of structural parameters derived from Reitveld refinement are significantly larger than these values. We have multiplied the esd's by a factor of 5 in quoting uncertainties of bond distances.

(23) (a) Manson, J. L.; Campana, C.; Miller, J. S. *J. Chem. Soc., Chem. Commun.* **1998**, 251−252. (b) Miller, J. S. *Adv. Mater.* **2001**, *13*, 525−527.
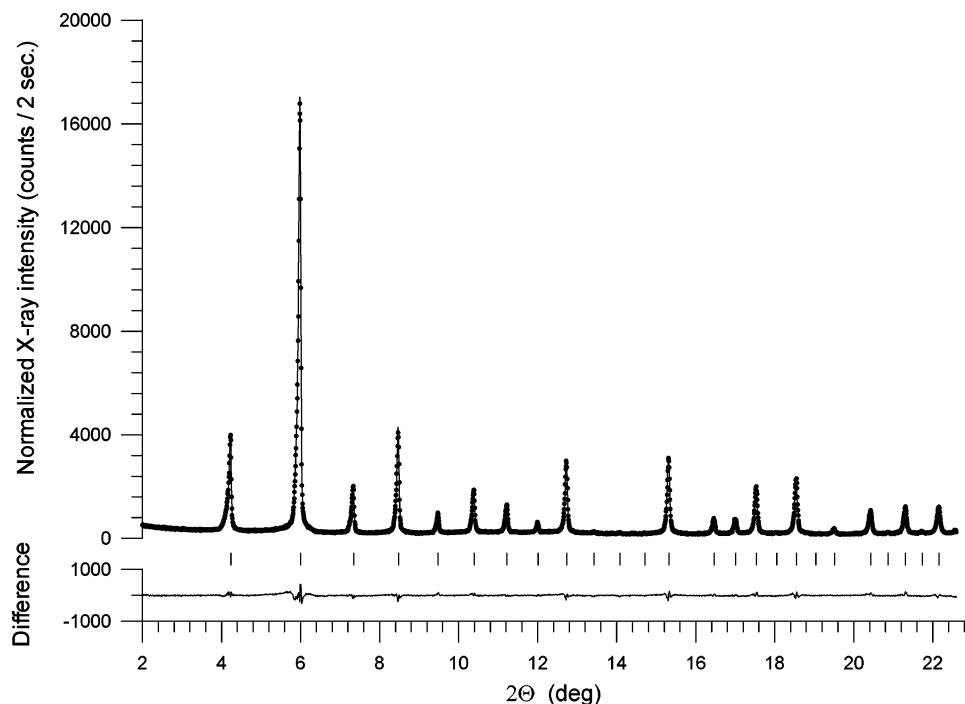
Figure 3. Reitveld fit to the Synchrotron powder diffraction data structure of **1a**. In the upper trace data points are denoted by filled circles, best Reitveld fit by a smooth curve. The vertical tick marks indicate positions of allowed Bragg peaks. The lower trace is the difference between the observed and calculated data on the same vertical scale.

Table 1. Summary of the Synchrotron Crystallographic Data for $[Ru_2(O_2CMe)_4]_3[Cr^{III}(CN)_6]$, **1a**

	$[Ru_2(O_2CMe)_4]_3[Cr^{III}(CN)_6]$, **1a**
formula	$C_{30}H_{36}CrN_6O_{24}Ru_6$
formula mass	1523.048
space group	$Im\bar{3}m$
a, Å	13.3756(5)
Z	2
V, Å^3	2392.9(3)
μ, cm^{-1}	16.6
ρ_{calcd}, g/cm^3	2.11
$R_{wp}{}^a$	0.0678
$R_{exp}{}^b$	0.0329
T, K	20 ± 2 °C
λ, Å	0.699 471

$^a R_{wp} = [\Sigma\, w(I_o - I_c)^2/\Sigma\, wI_o^2]^{1/2}$. $^b R_{exp} = [N_{obs} - N_{var}/\Sigma\, wI_o^2]^{1/2}$.

modeling reveals that when the carboxylic group is bigger than the acetic, e.g., propionic acid, a second interpenetrating lattice would be unexpected due to the large steric crowding between the two lattices. Therefore, the structure is expected to change from being a body-centered cubic structure to most likely a primitive cubic structure. Further studies are being done to explore the magnetic properties with different carboxylic groups.

The structure of $[Ru^{II/III}_2(O_2CMe)_4]_3[M^{III}(CN)_6]$ was not expected to change from changing from an aqueous (**1a**) to a nonaqueous synthesis route (**1b**). First, **1b** contains MeCN that is unexpected for an interpenetrating lattice structure. Unfortunately, **1b** did not diffract and was amorphous. The density of **1b** which was 1.90 g cm^{-3} does not correspond to a primitive cubic structure (1.06 g cm^{-3}) and is low for a interpenetrating lattice structure (2.11 g cm^{-3}). All samples prepared from nonaqueous media have low thermal stability, as evident by the broadening of the ν_{CN} in the IR spectrum, and their solvent content could not be determined by TGA due to the thermal decomposition. Elemental analysis showed that **1b** and **4** contained MeCN (4.6 and 8.1% of MeCN for **1b** and **4**,

respectively). Another alternative to a body-centered cubic structure for **1b** would be a 2-D structure similar to that observed for $[Ru_2(piv)_4]_3[Fe^{III}(CN)_6]\cdot4H_2O$.[3] The expected density of the 2-D structure would be similar to the primitive cubic structure, which is at variance to the observed density for **1b**.

Magnetic Properties. The magnetic susceptibilities, χ, of **1**−**4** were studied between 2 and 300 K at 50 Oe, and the 298 K effective moments, μ_{eff} [$=(8\chi T)^{1/2}$], for **1a**, **1b**, **2**, **3**, and **4** are 7.72, 7.23, 7.30, 7.26, and 7.53 μ_B, respectively (Figure 4). The room-temperature moment for **1a**, **1b**, **2**, **3**, and **4** are close to the expected spin-only value of 7.75, 6.93, 6.71, and 7.28 μ_B for **1**, **2**, **3**, and **4**, respectively. Fitting $\mu_{eff}(T)$ data with a model expression is more complex than using the classic Curie−Weiss equation, since $[Ru^{II/III}_2(O_2CR)_4]^+$ is known to have a large zero-field splitting (*D*) and temperature-independent paramagnetism (TIP).[4,5] Their contribution to $\chi(T)$ was incorporated into eq 1,[3,7,24] and eqs 1−3 were used to model $\mu_{eff}(T)$ for **1**−**4**. The Weiss constant, θ, was introduced to account for magnetic interactions between the paramagnetic species. A summary of the magnetic properties are presented in Table 2.

$$\chi_{Ru_2} = \frac{Ng^2\mu_B^2}{k_B(T-\theta)}\left[\frac{1}{3}\cdot\frac{1+9e^{-2D/k_BT}}{4(1+e^{-2D/k_BT})} + \frac{2}{3}\cdot\frac{1+\dfrac{3k_BT}{4D}(1-e^{-2D/k_BT})}{1+e^{-2D/k_BT}}\right] + TIP \text{ for } T > \theta \quad (1)$$

$$\chi_M = \frac{Ng^2\mu_B^2}{3k_B(T-\theta)}[S(S+1)] \quad (2)$$

$$\chi_{Tot} = 3\chi_{Ru_2} + \chi_M \quad (3)$$

While the IR spectra of $[Ru^{II/III}_2(O_2CMe)_4]_3[Cr^{III}(CN)_6]$ syn-

Table 2. Summary of the ν_{CN} IR Absorptions and Magnetic Properties for $[Ru_2(O_2CMe)_4]_3[M^{III}(CN)_6]$

	M	ν_{CN} cm^{-1}	T_c, K	T_b, K	M_s,[b] emu Oe/mol	M_s (calcd)[c] FO emu Oe/mol	M_s (calcd)[c] AF emu Oe/mol	M_r emu Oe/mol	ϕ^d	H_{cr} Oe
1a	Cr	2138	33	32	$20\,800 \pm 300$	67 020	33 510	3840	<0.001	470
1b	Cr	2142	34.5	32	$16\,000 \pm 700$	67 020	33 510	8830	<0.001	1670
2	Fe	2116	2.1	3	$22\,700 \pm 400$	55 850	44 680	40	<0.001	10
3	Co	2125			31 125	50 265	50 265			
4	Mn	2118	9.6	10	$20\,000 \pm 600$	61 435	39 095	7170	0.008	990

[a] Temperature range fit with eq 3. [b] M_s is the magnetization at 5 T at 2 K (Figure 7). [c] Equation 5. [d] Equation 4.

Figure 4. $\mu_{eff}(T)$ for **1**–**4** and the fit to the high-temperature data with eq 3 as the solid blue lines.

thesized via an aqueous route (**1a**) and MeCN route (**1b**) are nearly identical suggestive of similar structures, the magnetic data differ significantly. Similar dependence on the solvent on the magnetic properties has been observed for some Prussian blue compounds.[18] The $\mu_{eff}(T)$ of **1a** and **1b** are nearly identical

above 50 K (Figure 4 top) before $\mu_{eff}(T)$ and increases with decreasing temperature to maximum values of 31 μ_B at 32 K for **1a** and 112 μ_B at 33 K for **1b** before abruptly decreasing to 3.65 μ_B for **1a** and 12.0 μ_B for **1b** at 2 K. $\mu_{eff}(T)$ for **1a** and **1b** above 120 K were fit with eq 3 with $D = 69.4$ cm^{-1}, $\theta = -40$ K, $g_{Ru2} = 2$, $g_{Cr} = 2$, and $TIP_{Ru2} = 700 \times 10^{-6}$ emu mol^{-1} (χ^2 agreement factor[25] $= \Sigma(\mu_{exp} - \mu_{calc})^2/\mu_{exp} = 5.51 \times 10^{-3}$) for **1a** and $D = 69.4$ cm^{-1}, $\theta = -70$ K, $g_{Ru2} = 2$, $g_{Cr} = 2$, and $TIP_{Ru2} = 500 \times 10^{-6}$ emu mol^{-1} ($\chi^2 = 1.31 \times 10^{-4}$) for **1b**. The TIP values are in good agreement with others reported.[6,7,8]

Magnetic ordering of **1a** and **1b** was ascertained from the low-field magnetization, $M(T)$, as well as zero-field cooled (ZFC) and field cooled (FC) $M(T)$ studies. Magnetic ordering may result in a bifurcation point between the ZFC and FC $M(T)$ data, Figure 5. The observed difference between the ZFC and FC data for **1a** is small but reproducible with a bifurcation point of 32 K. Magnetic ordering of **1a** and **1b** was confirmed from the real, in-phase (χ') and imaginary, out-of-phase (χ'') alternating current (AC) susceptibilities, Figure 6. **1a** has frequency independent peaks for both $\chi'(T)$ at 32 K and $\chi''(T)$ at 34 K.

The AC and ZFC–FC magnetic data for **1b** differ more than those for **1a**. **1b** has frequency independent peaks for both $\chi'(T)$ at 34.5 K and $\chi''(T)$ at 34 K. Unlike **1a**, however, the width of the $\chi'(T)$ peak was narrow. Also, the ZFC and FC data had a very distinct bifurcation point at 32 K indicating magnetic ordering. Removal of MeCN from **1b** results in reduced T_c's and a frequency dependence for $\chi'(T)$ and $\chi''(T)$ indicating disorder in the desolvated structure.

For **2**, $\mu_{eff}(T)$ is fairly constant with decreasing temperature until it sharply increases at ~10 K reaching 19.2 μ_B at 2 K. Data above 15 K was fit with eq 3 with $D = 69.4$ cm^{-1}, $\theta = 0$ K, $g_{Ru2} = 2.0$, $g_{Fe} = 3.0$, and $TIP_{Ru2} = 300 \times 10^{-6}$ emu mol^{-1} ($\chi^2 = 2.22 \times 10^{-3}$). The divergence in the ZFC data and the FC data at 3 K suggests a transition from short-range ferromagnetic interaction to long-range ferromagnetic ordering. **2** has frequency independent peaks for both $\chi'(T)$ at 2.1 K and $\chi''(T)$ at 2.1 K.

$[Co^{III}(CN)_6]^{3-}$ of **3** is diamagnetic, and therefore, the only magnetic site in **3** is that of $[Ru^{II/III}_2(O_2CR)_4]^+$. Thus, $\mu_{eff}(T)$ for **3** was fit by eq 3 with $D = 69.4$ cm^{-1}, $TIP_{Ru2} = 800 \times 10^{-6}$ emu mol^{-1}, $\theta = 0$ K, $g_{Ru2} = 2.04$ (Figure 4) above 4 K. This is in good agreement with other salts of $[Ru^{II/III}_2(O_2CR)_4]^+$ with diamagnetic anions.[7]

For $[Ru^{II/III}_2(O_2CMe)_4]_3[Mn^{III}(CN)_6]$ (**4**), $\mu_{eff}(T)$ increases sharply with decreasing temperature below ~20 K and reaches a maximum of 67 μ_B at 11 K, prior to decreasing to 9 μ_B at 2 K. Above 60 K, $\mu_{eff}(T)$ was fit with eq 3 with $D = 69.4$ cm^{-1}, $\theta = -20$ K, $g_{Ru2} = 2.0$, $g_{Mn} = 2.0$, and $TIP_{Ru2} = 270 \times 10^{-6}$

(24) O'Connor, C. J. *Prog. Inorg. Chem.* **1982**, *29*, 203–283.

(25) Taylor, J. *An Introduction to Error Analysis*: University Science Books: Mill Valley, CA, 1982; pp 218–223.
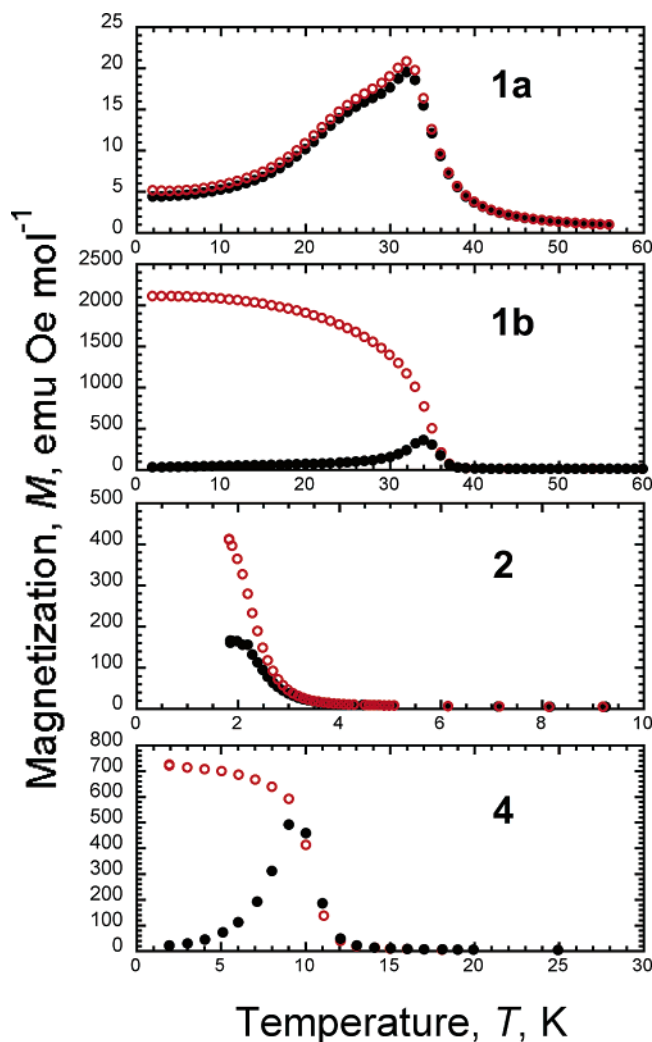
Figure 5. Field cooled (FC, ○) and zero field cooled (ZFC, ●) $M(T)$ data for **1a**, **1b**, **2**, and **4**.

emu mol^{-1} ($\chi^2 = 8.51 \times 10^{-3}$). The AC susceptibility data of **4** contained a slight frequency-dependent $\chi'(T)$ peak at 9.6 K at 10 Hz and $\chi''(T)$ peak at 9.5 K at 10 Hz. If **4** was not freshly prepared or dried under vacuum, the AC susceptibility peaks shifted to lower temperature and had a large frequency dependence indicating a disordered spin glass structure. This is attributed to some decomposition.

$$\phi = \Delta T_f / [T_f \Delta(\log f)] \tag{4}$$

The frequency dependence in the $\chi'(T)$ can be parametrized by ϕ,[26] where T_f is the temperature of the peak in the lowest frequency (10 Hz) data, f, the frequency in Hz, and the greater the frequency dependence the larger the value of ϕ (*i.e.,* the greater the spin glass behavior). The ϕ of 0.008 for **4** is on the low end of disordered spin systems, which display ϕ values that typically range from 0.01 to 0.1 such as those found in the alloys of *Pd*Mn, 0.013 and *Ni*Mn, 0.018, and the superparamagnet α-(Ho$_2$O$_3$)(B$_2$O$_3$), 0.28.[26] The data for crystalline **1a**, as well as freshly prepared **1b** and **4**, do not have a significant frequency dependence and consequently do not show spin glass behavior. In contrast, solvated **1b** and **4** display spin glass

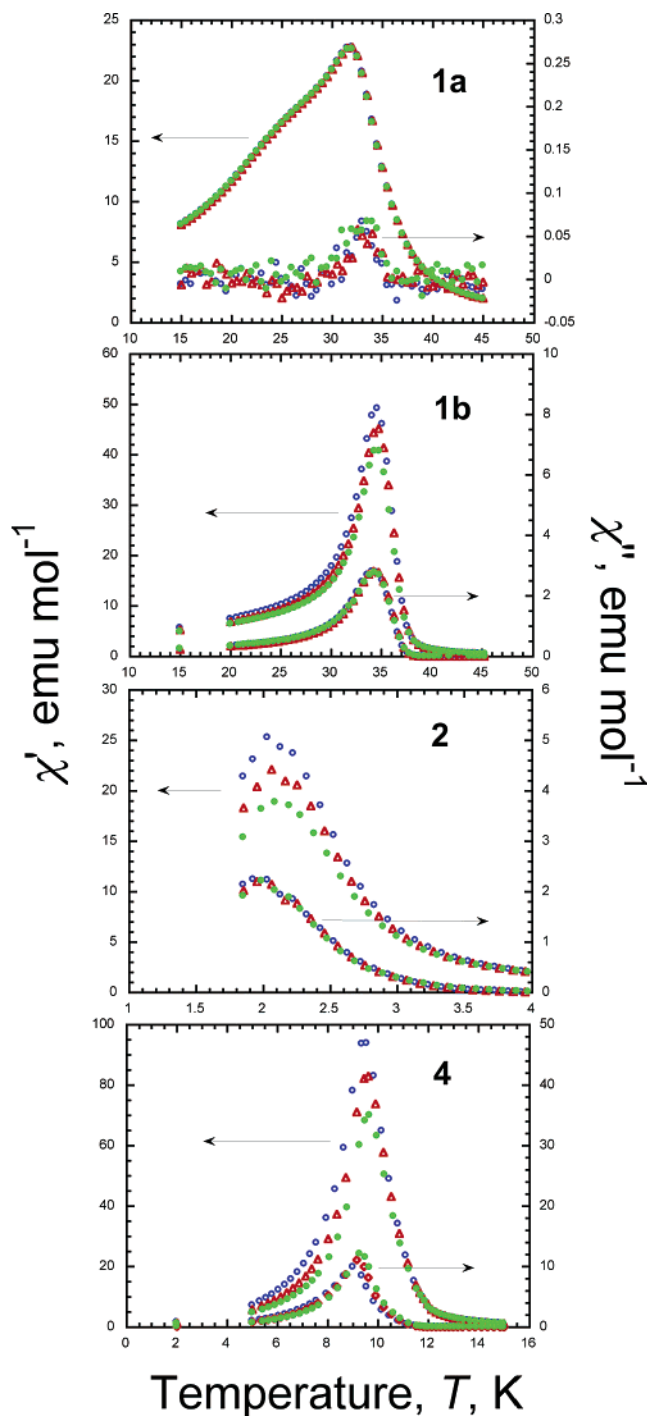(26) Mydosh, J. *Spin Glasse*s; Francois and Taylor: 1993; pp 64–76.

Figure 6. AC $\chi'(T)$ and $\chi''(T)$ at 10 (blue o), 100 (red Δ), and 1000 (green λ) Hz for **1a**, **1b**, **2**, and **4**.

behavior upon drying under vacuum at room temperature. This is attributed to the breakdown of a long-range 3-D structure upon the loss of MeCN. This could also be the factor that initiates the thermal decomposition.

The field dependence of the magnetization, $M(H)$, for $[Ru^{II/III}{}_2(O_2CR)_4]^+$ cannot be fit to the Brillouin function due the presence of the large zero-field splitting, D (+53 ± 24 cm^{-1}),[5b,6] as the $M(H)$ is measured at 2 K ($k_BT \ll D$) and the $m_s = \pm^1/_2$ state is essentially solely populated. Hence, the saturation magnetization, M_s, is much lower than the expected value using eq 5.[27] For example, an M_s of 33 500 emu Oe mol^{-1} is expected for antiferromagnetic coupling for **1**, while 20 800
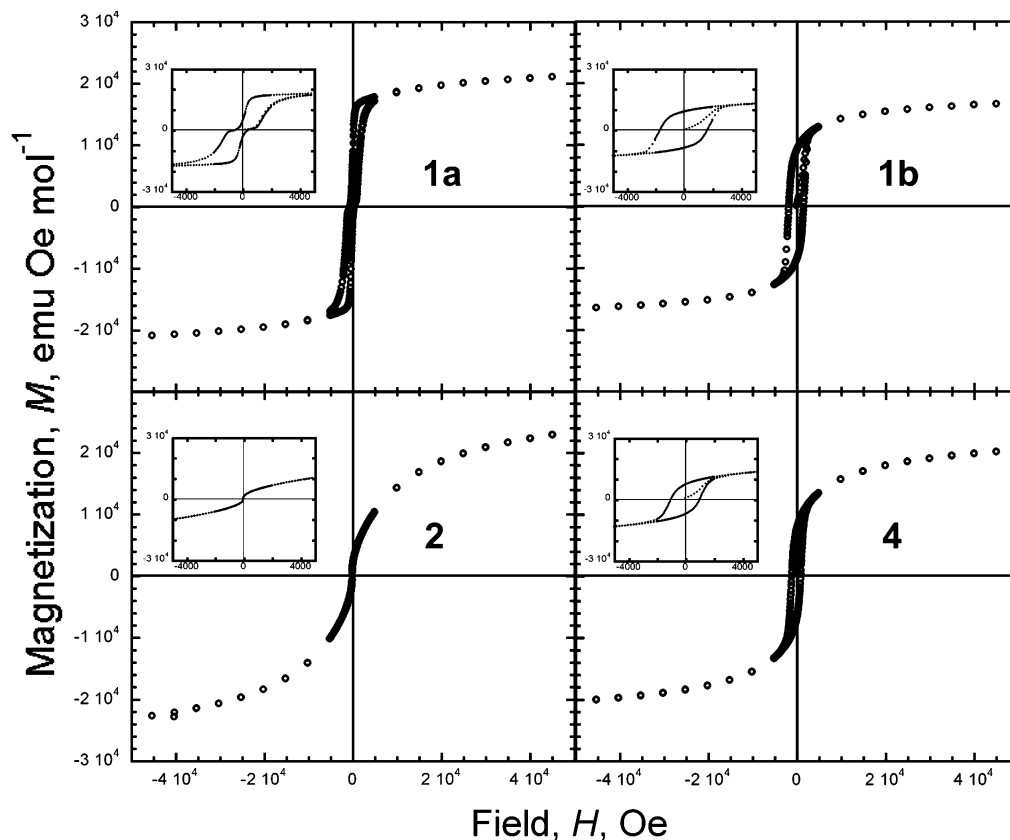
Figure 7. $M(H)$ of **1a**, **1b**, **2**, and **4** at 2 K taken from $\pm50\,000$ Oe. Inserts highlight the region from ±5000 Oe.

emu Oe mol^{-1} was observed. An analytical expression for the anisotropic magnetization of $S = {}^3/_2$ as a function of D is yet to be reported. The effect of zero-field splitting (D) on the $M(H)$ data is currently under further investigation.

$$M_s = Ng\mu_B(3S_{Ru2} \pm S_{Cr}) \tag{5}$$

While the values of the saturation magnetizations are not easily analyzed due to the zero-field splitting, the asymptoting magnetization of **1a** (20 800 emu Oe mol^{-1}) and **1b** (16 000 emu Oe mol^{-1}) at 5 T and 2 K are significantly different. The different asymptoting $M(H)$ of **1a** and **1b** at 5 T and 2 K were reproducible, and the difference could not be accounted for by solvent in the structure of **1b**. The differences in magnetization between **1a** and **1b** are possibly attributed to different solid-state structures obtained from the aqueous compared to MeCN synthetic route. Since the structure of **1b** has not been obtained, the structural correlation to the magnetic data is not readily apparent but may arise from spin canting to different degrees.

The $M(H)$ data at 2 K showed a very unusual constricted hysteresis loop for **1a** with a coercive field, H_{cr}, of 470 Oe, Figure 7. The unusual constricted hysteresis loop for **1a** was reproducible between several independently made samples. Constricted hysteretic behavior, albeit qualitatively different, has been attributed to metamagnetism caused by canted spins,[21e] and this phenomenon is under further study. The remnant magnetization for **1a** at 2 K is 3800 emu Oe mol^{-1}. Only crystalline **1a** has an unusual constricted hysteresis loop in the $M(H)$ data at 2 K. Surprisingly, the $M(H)$ data of the analogous

material made in acetonitrile, **1b**, did not have this constricted hysteresis loop but contained a classical hysteresis loop. The reasons for the different magnetic data between **1a** and **1b** are still under investigation. **1b**, **2**, and **4** exhibit normal, noncon-stricted hysteresis with coercive fields of 1670, 10, and 990 Oe, respectively.

^{57}Fe Mössbauer Spectroscopy. The temperature dependence of the ^{57}Fe Mössbauer spectrum of **2** confirms the presence of a single iron-containing species, Figure 8. The small, negative ambient temperature isomer shifts (δ) of -0.05 mm/s and small quadrupole spitting (ΔE) of 0.33 mm/s of **2** are typical of low-spin Fe^{III} in ferricyanides, e.g., K$_3$[Fe(CN)$_6$] ($\delta = -0.124$ mm/s, $\Delta E = 0.280$ mm/s).[28] The isomer shift for **2** is 0.07 mm/s more positive than that of K$_3$[Fe(CN)$_6$] reflecting an increased level of d electron delocalization from the [Ru$^{II/III}_2$(O$_2$CR)$_4$]$^+$ dimer to [Fe(CN)$_6$]$^{3-}$, and concomitant increase in "s" electron shielding at the low-spin Fe^{III} centers. At lower temperatures, a transition from the rapidly relaxing (unordered) paramagnetic state to the onset of 3-D magnetic ordering is evident. This is consistent with the observed sharp rise in moment to ~19 μ_B at 2 K (Figure 4), bifurcation at low-temperature ZFC/FC $M(T)$ data (Figure 5), absorptions in the $\chi'(T)$ and $\chi''(T)$ data (Figure 6), and hysteresis at 2 K (Figure 7). At 1.2 K (the low-temperature limit for our ^{4}He cryogenics system), critical spin fluctuations are apparently still sufficiently important as to lead to a highly broadened hyperfine pattern instead of the classical, resolved, narrow line-width, six transition pattern expected for magnetic saturation. The latter is observed for [Fe(CN)$_6$]$^{3-}$,[29] which orders at ~0.129 K with an internal field, $H(0\ K)$, of

(27) Carlin, R. L. *Magnetochemistry*; Springer-Verlag: Berlin Heidelberg, 1986; Chapter 1.

(28) Greenwood, N. N.; Gibb, T. C. *Mössbauer Spectroscopy*; Chapman and Hall Ltd.: London, 1971; p 174.
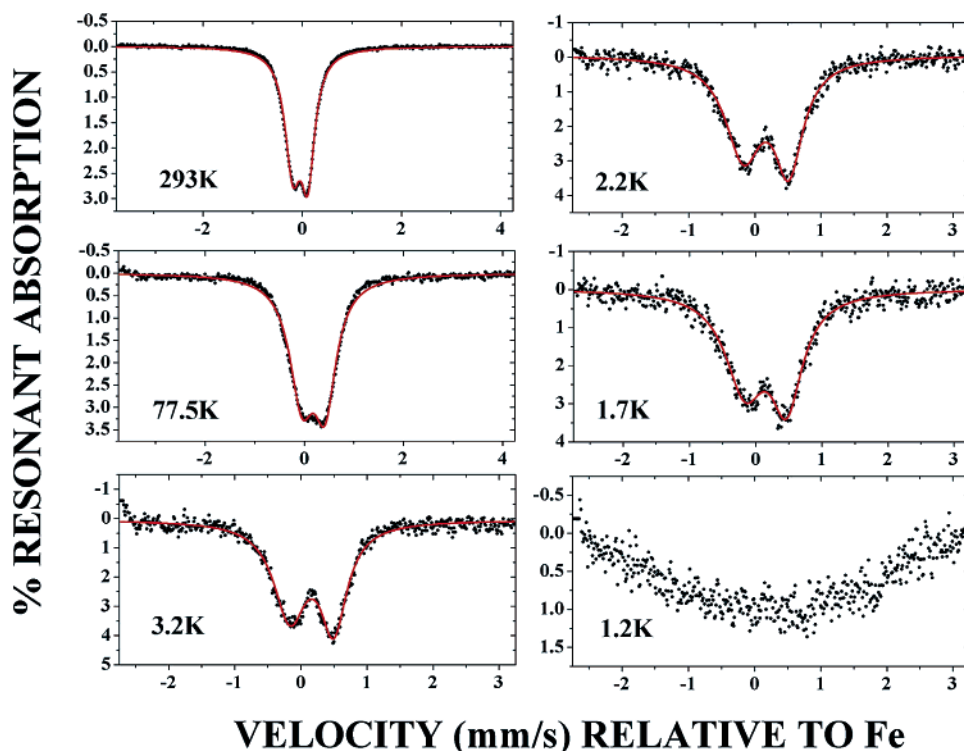
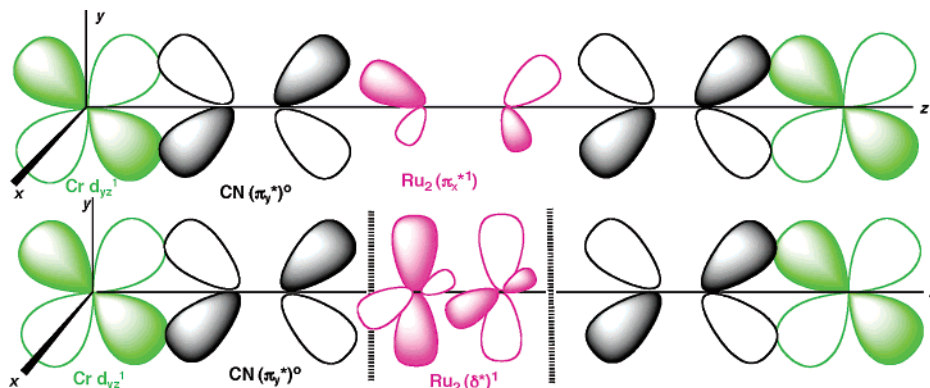**Figure 8.** Temperature dependence of the ^{57}Fe Mössbauer spectra of **2**.

Figure 9. Nearest neighbor overlap in the xz plane for a ···Cr−CN−Ru$_2$−NC−Cr··· segment (45° relative rotation): depicting the nonorthogonal overlap of the Cr^{III} d$_{yz}$, CN π_y*, and Ru$_2$ π_y* orbitals (the degenerate nonorthogonal overlap of the Cr^{III} d$_{yz}$, CN π_y*, and Ru$_2$ π_x* or Cr^{III} d$_{xz}$, CN π_x*, and Ru$_2$ π_x* orbitals etc. are not shown) (top) and depicting the nonbonding orthogonal overlap of the Cr^{III} d$_{yz}$, CN π_y*, and Ru$_2$ δ* orbitals (the degenerate orthogonal overlap of the Cr^{III} d$_{xz}$, CN π_x*, and Ru$_2$ δ* orbitals is not shown) (bottom).

194 kOe corresponding to a hyperfine splitting of ~6.25 mm/s, which is comparable to the velocity span of the broad absorption pattern at 1.2 K. The Mössbauer spectroscopy results imply a $T_c \approx 1.5$ K for **2**, an order of magnitude greater than that found K$_3$Fe(CN)$_6$],[29] which contains "isolated" [Fe(CN)$_6$]$^{3-}$ ions.

Nearest Neighbor Spin Coupling (J) and Critical Temperature (T_c). The orbital overlap of the singly occupied molecular orbitals (SOMOs) was qualitatively analyzed to interpret the antiferromagnetic coupling between metal ions for the [Ru$_2$(O$_2$CMe)$_4$]$_3$[M^{III}(CN)$_6$] family of magnets. If these SOMOs are orthogonal ferromagnetic coupling is expected; otherwise, antiferromagnetic coupling is expected.[1e,30a] This analysis for the observed [Ru$_2$(O$_2$CMe)$_4$]$_3$[Cr^{III}(CN)$_6$] structure

(Figure 2) is illustrated in Figure 9 for the overlap of a Cr^{III} t$_{2g}$ (d$_{xz}$, d$_{yz}$, and d$_{xy}$) SOMO with the cation's δ*$^1\pi$*^{2} (derived from the overlap of the d$_{xy}$, d$_{xz}$, and d$_{yz}$ orbitals on each Ru, respectively) singly occupied orbitals in the xy plane. Overlap of the Cr^{III} t$_{2g}$ d$_{yz}$^{1} (as well as the degenerate d$_{xz}$^{1}) and Ru$_2$ π_y*^{1} (as well as the degenerate π_x*^{1}) orbitals is nonorthogonal; thus, antiferromagnetic coupling is expected, Figure 9 top. This overlap is a two-electron three-orbital interaction akin to that invoked to explain the three-center two-electron BHB bonding in diborane. In contrast, overlap of the Cr^{III} t$_{2g}$ d$_{yz}$ (as well as

(29) (a) Shinohara, M.; Ishigaki, A.; Ono, K. *Jpn. J. Appl. Phys.* **1968**, *7*, 170−173. (b) Groves, J. L.; Becker, A. L.; Chirovsky, L. M.; Lee, W. P.; Wang, G. W.; Wu, C. S. *Hyperfine Interact.* **1978**, *4*, 930−941.

(30) (a) Verdaguer, M.; Bleuzen, A.; Marvaud, V.; Vaissermann, J.; Seuleiman, M.; Desplanches, C.; Scuiller, A.; Train, C.; Garde, R.; Gelly, G.; Lomenech, C.; Rosenman, I.; Veillet, P.; Cartier, C.; Villain, F. *Coord. Chem. Rev.* **1999**, *190−192*, 1023−1047. (b) Tanaka, H.; Okawa, N.; Kawai, T. *Solid State Commun.* **1999**, *110*, 191−196. (c) Greedan, J. E.; Chien, C.-L.; Johnston, R. G. *J. Solid State Chem.* **1976**, *19*, 155−160. (d) Greedan, J. E. *J. Phys. Chem. Solids* **1971**, *32*, 819−823. (e) Kimishima, Y.; Ichiyanagi, Y.; Shimizu, K.; Mizuno, T. *J. Magn. Magn. Mater.* **2000**, *210*, 244−250.

Table 3. T_c Ratio from Experiment and Theoretical Calculation (Assuming Same J for **1a**, **2**, and **4**)

	exp ratio	two-spin site mean field[a] $S_{Ru2} - S_M$	two-spin site mean field[a] $S_{eff}(T) - S_M$	ZFS[b], anisotropic spin distribution $- S_M$
1a/2	15.7	2.24	2.45	2.45
4/2	4.6	1.63	1.67	1.67
2/2	1	1	1	1

[a] Equation 6. [b] Equation 7.

Table 4. J Values Calculated from Experimental T_c's

	$|J|/k_B$ from ZFS,[a] anisotropic spin distribution $- S_M$	$|J|/k_B$ from two-spin site mean field[b] $S_{eff}(T) - S_M$
1a	4.46 K	4.46 K
4	1.90 K	1.90 K
2	0.70 K	0.70 K

[a] Values calculated from eq 7. [b] Values calculated from eq 6.

the degenerate d_{xz}) and Ru_2 fragment's δ^* is nonbonding/orthogonal, Figure 9 bottom, and ferromagnetic coupling is expected. The competition between ferro- and antiferromagnetic couplings results in the antiferromagnetic coupling being dominant, as noted for several members of the Prussian blue structured magnets.[30] Consequently, ferrimagnetic, not ferromagnetic, ordering is expected, as is observed for the $[Ru_2(O_2CMe)_4]_3[M^{III}(CN)_6]$ family of magnets. This model suggests that utilization of $S = \frac{1}{2}$ $[M_2(O_2CR)_4]^+$ with a δ^{*1} electronic structure should couple ferromagnetically. Further studies are being done on $Rh^{II/III}_2$ cations[31] that have this electronic structure. Likewise, the same analysis leads to the identical conclusion if the cation had a $\pi^2\delta^1$ electronic structure; thus $S = \frac{1}{2}$ $[M_2(O_2CR)_4]^+$ and related cations with a δ^1 electronic structure, e. g., $[Mo_2(2,4,6-C_6H_2Pr^i_3CO_2)_4]^+$ [32a] and $[V_2(DPhF)_4]^+$ (DPhF = N,N'-diphenylformamide anion),[32b] should couple ferromagnetically.[33]

One expression that has proved useful in the analysis of the nearest neighbor spin exchange, J, of T_c's in Prussian blue and perovskite structures was obtained from Néel's equation[30,34]

$$T_c = \frac{2z|J|\sqrt{S_{Ru2}(S_{Ru2}+1)S_M(S_M+1)}}{3k_B} \quad (6)$$

where k_B is the Boltzmann constant, z is number of the nearest neighbors equals to $[z_{Ru}z_M]^{1/2}$, and J is the coupling between nearest neighbor M and Ru sites. The T_c's for a family of Prussian blue and perovskite structured magnets have been analyzed using Neel's expression, eq 6.[30] Qualitatively, the T_c's of $[Ru_2(O_2CMe)_4]_3[M^{III}(CN)_6]$ follows the trend expected in eq 6 as the greater number of unpaired spins on the $[M^{III}(CN)_6]^{3-}$ (Fe < Mn < Cr) results in a larger T_c with everything else being equal. Assuming J is constant, as occurs for the comparison of $[M(C_5Me_5)_2][TCNE]$ [M = Fe ($S = \frac{1}{2}$), Mn ($S = 1$)],[35] the relative T_c's for **2:4:1a** are 1:1.63:2.24 from eq 6, Table 3. This

is substantially lower than the experimental ratio of 1:4.6:15.7. While eq 6 is appropriate for a two-spin system, this model does not take into account the effects of the spin anisotropy from zero-field splitting for the $[Ru_2(O_2CMe)_4]^+$.

The effect of the spin anisotropy for the $[Ru_2(O_2CMe)_4]^+$ was accounted for in two different ways. First, when there is no coupling between two $[Ru_2(O_2CMe)_4]^+$, the $\mu_{eff}(T)$ differs from the spin-only value due to zero-field splitting. An effective spin, S_{eff}, for $[Ru_2(O_2CMe)_4]^+$ was obtained from a model compound with essentially no coupling between diruthenium sites, i.e., **3**. From the $\mu_{eff}(T)$ for **3**, $S_{eff}(T)$ values for $[Ru_2(O_2CMe)_4]^+$ at the T_c's for **2** (2.1 K), **4** (9.6 K), and **1a** (33 K) are 1.09, 1.13, and 1.23, respectively. Using S_{eff} in place of S_{Ru2} in eq 6, the relative T_c's are calculated to be 1:1.67:2.45 (Table 3), which was only slightly increased than from when using $S_{Ru2} = \frac{3}{2}$.

Second, the spin anisotropy for $[Ru_2(O_2CMe)_4]^+$ from the zero-field splitting (D) was directly accounted for in the T_c calculation from a modified simple mean-field model (eq 7), where D is the zero-field splitting. Again assuming J was constant, the relative T_c's were calculated from eq 7 and found to be 1:1.67:2.45 for Fe(**2**):Mn(**4**):Cr(**1a**) (Table 3), which are identical to the relative T_c's from eq 6 using $S_{eff}(T)$. The zero-field splitting model, eq 7,

$$T_c = \frac{2\sqrt{z_{Ru2}z_M}|J|\sqrt{F(D,T,S_M)}}{3k_B};$$

$$F(D,T,S_M) =$$

$$3\left[\frac{1}{3}\frac{1+9e^{-2D/k_BT}}{4(1+e^{-2D/k_BT})} + \frac{2}{3}\frac{1+\frac{3k_BT}{4D}(1-e^{-2D/k_BT})}{1+e^{-2D/k_BT}}\right] \cdot$$

$$S_M(S_M+1) \quad (7)$$

accounts for the spin anisotropy due to zero-field splitting directly, while the two-site, mean-field model, eq 6, accounts for the spin anisotropy with S_{eff}.[36]

Since the relative T_c's from eqs 6 and 7 assuming constant J values do not equal the experimental T_c's, the J values for **1a**, **2**, and **4** were calculated using eqs 6 and 7, Table 4. The calculated J values follow the trend of $J(\mathbf{2}) < J(\mathbf{4}) < J(\mathbf{1a})$.

Conclusion

The magnetic properties of a series of $[Ru_2(O_2CMe)_4]_3[M^{III}(CN)_6]$ compounds were systematically studied, and the ruthenium dimer monocations can be utilized as building blocks for molecule-based magnets. The properties of the molecule-based magnets are dependent on the reaction conditions; nonaqueous

(31) For example, see: (a) Ren, T. *Coord. Chem. Rev.* **1998**, *175*, 43−58. (b) Kadish, K. M.; Phan, T. D.; Giribabu, L.; van Caemelbecke, E.; Bear, J. L. *Inorg. Chem.* **2003**, *42*, 8663−8670.
(32) (a) Cotton, F. A.; Daniels, L. M.; Hillard, E. A.; Murillo, C. A. *Inorg. Chem.* **2002**, *41*, 1639−1644. (b) Cotton, F. A.; Hillard, E. A.; Murillo, C. A.; Wang, X. *Inorg. Chem.* **2003**, *42*, 6063−6070.
(33) This analysis is for the observed structure with the $[Ru_2(O_2CMe)_4]^+$ paddlewheel being rotated 45° with respect to the octahedral $[M(CN)_6]^{3-}$ (to accommodate the second, interpenetrating lattice), but this relative rotation may not occur for other structures, especially those lacking an interpenetrating second lattice. Analysis of the overlap of the Cr^{III} t_{2g} $d_{yz}{}^1$ and Ru_2 fragment's π_y^{*1} (as well as the former's degenerate π_x^{*1} and the latter's degenerate π_x^{*1}) is nonorthogonal; hence, antiferromagnetic coupling is expected. In contrast, overlap of the Cr^{III} t_{2g} d_{yz} (as well as the degenerate d_{xz}) with the Ru_2 fragment's δ^* is nonbonding/orthogonal, and ferromagnetic coupling is expected. As in the 45° relative rotation case described in the text, the competition between ferro- and antiferromagnetic couplings should result in the antiferromagnetic coupling dominating.
(34) Néel, L. *Ann. Phys. (Paris)* **1948**, *3*, 137−198.
(35) Dixon, D. A.; Suna, A.; Miller, J. S.; Epstein, A. J. In *Magnetic Molecular Materials*; Gatteschi, D., Kahn, O., Miller, J. S., Palacio, F., Eds.; Kluwer Academic Publishers: Boston, MA, 1991; E198, 171−190.

(36) While eqs 6 and 7 appear different, both models are based on mean field theory and eq 7 becomes identical with eq 6 when D approaches 0.

and aqueous routes provided different magnetic materials for [Ru$_2$(O$_2$CMe)$_4$]$_3$[Cr^{III}(CN)$_6$] as has been observed for Prussian blue structured magnets. The 2-D structured [Ru$_2$(piv)$_4$]$_3$[Fe^{III}-(CN)$_6$]·4H$_2$O[3] had an upturn in $\mu_{eff}(T)$ at ∼8 K similar to what we observed for [Ru$_2$(O$_2$CMe)$_4$]$_3$[M^{III}(CN)$_6$] (M = Cr, Fe, and Mn), and further studies could provide evidence of magnetic ordering. The magnetic properties and solid-state structure can be tuned by modifying the metal hexacyanide. The T_c's for **1**, **2**, and **4** followed the trend of increasing with increasing spin on the metal hexacyanide, but they increase to a greater extent than can be accounted for from mean-field theory without changing the J values. Novel magnetic behaviors may be achieved by utilizing the extraordinary large zero-field splitting.

Supporting Information Available: X-ray CIF files for [Ru$_2$(O$_2$CMe)$_4$]$_3$[Cr^{III}(CN)$_6$], **1a**, has been deposited with the Cambridge Crystallographic Data Center, Ref No. CCDC-234876. This material is available free of charge via the Internet at http://pubs.acs.org.

JA048135I